Reduction of Thermal Conductivity in Silicene Nanomesh: Insights from Coherent and Incoherent Phonon Transport

Liu Cui [1, 2, †], Sanqiang Shi [2], Zhao Li [1], Gaosheng Wei [1], Xiaoze Du [1, †]

[1] *Key Laboratory of Condition Monitoring and Control for Power Plant Equipment, Ministry of Education, North China Electric Power University, Changping, Beijing 102206, China*

[2] *Department of Mechanical Engineering, The Hong Kong Polytechnic University, Hung Hom, Kowloon, Hong Kong, China*

[†] To whom correspondence should be addressed.

E-mail: liucui@ncepu.edu.cn (L. Cui); duxz@ncepu.edu.cn (X. Du)

Abstract

Silicene nanomesh (SNM), a silicene sheet with periodically arranged nanoholes, has gained increasing interest due to its unique geometry and novel properties. In this paper, we have conducted molecular dynamics simulations to study the phonon transport properties of SNMs. The results demonstrate that the thermal conductivity of SNM, which is shown to be much lower than that of silicene, is little affected by temperature but can be effectively tuned by varying the porosity. To elucidate the underlying mechanisms for decreased thermal conductivity, we have investigated both coherent and incoherent phonon transport in SNMs. It is found that the phonon backscattering at the nanopore edges leads to extra thermal resistances. Additionally, the introduction of nanopores induces phonon localization and consequently hinders phonon transport in SNMs. The phonons of SNM exhibit coherent resonant behavior, which is believed to reduce the phonon group velocities and thus leads to a further reduction in thermal conductivity of SNMs. Our findings could be useful in the design of thermal properties of silicene for applications in thermoelectrics, thermal insulation and thermal protection.

1. Introduction

Since its experimental isolation in 2004 [1], graphene has been the focus of extensive research due to its excellent heat transfer properties [2, 3], which make it attractive for heat dissipation applications. Inspired by the advances in graphene, many other two-dimensional (2-D) materials [4, 5], such as hexagonal boron nitride, silicene, black phosphorus and molybdenum disulfide, have been synthesized and studied. Among them, silicene is one of the most promising materials because of its compatibility with current silicon-based semiconductor devices [6, 7]. Similar to graphene, silicene is composed of a single layer of atoms arranged in a 2-D honeycomb lattice. However, the larger atomic radius of silicon promotes sp^3 hybridization in silicene, while sp^2 hybridization is more favorable in graphene [8, 9]. Different from the planar structure of graphene, the honeycomb lattice of silicene is slightly buckled. Due to the similarities and differences between the lattice structures of silicene and graphene, it is of great interest to explore the thermal transport in silicene-based materials.

Patterning a graphene or silicene sheet into a nanomesh structure (i.e. a 2-D sheet with periodically arranged nanopores) can modify and tune its electronic and electrical properties [10-13]. It has been reported that graphene nanomeshes (GNMs) containing a specific nanohole can tune between metallic and semiconducting states, as well as a semimetal state [12]. A first-principles study has shown that a band gap is opened in silicene nanomeshes (SNMs) and the size of the band gap increases with the reduced neck width [10]. Recently, the effect of nanopores on the thermal conductivity of planar graphene has been widely investigated. Feng and Ruan [14] found that the thermal

conductivity of GNM is more than 3 orders of magnitude lower than that of the pristine graphene [14], which leads to new applications of graphene in thermoelectrics. Yang et al. [15] reported that the increase of porosity enhances phonon localizations in GNMs, which results in the reduction of thermal conductivity. Yarifard et al. [16] showed that the porosity, periodicity, neck width and the geometry of nanoholes can be used to tune the thermal conductivity of GNM. However, in contrast to the extensive investigations on heat transfer in GNM, little is known about how periodic nanopores affect the thermal conductivity of silicene. It is interesting to know whether nanopores have the same impact on thermal conductivities of silicene and graphene. On the other hand, SNMs can be viewed as 2-D superlattices constructed from periodic nanopores. It has been widely debated whether the coherent phonon transport could occur in the superlattices. The underlying physical mechanisms of SNMs in view of the coherent and incoherent phonon transport need to be further investigated.

Motivated by these issues, in this work, we study the thermal conductivity of SNM by using nonequilibrium molecular dynamics (NEMD) simulations. Our results confirm that, similar to that of graphene, the thermal conductivity of silicene can be suppressed by introducing nanopores. However, the thermal conductivity reduction ratio in silicene is less than that in graphene. In addition, the temperature and porosity effects on the thermal conductivity of SNM were studied. By analyzing the temperature distribution, phonon lifetime, phonon participation ratio and mode weight factor, both coherent and incoherent phonon transport in SNMs were investigated. It is found that the introduction of nanoholes induces the phonon backscattering, phonon localization and phonon

coherent resonance.

2. Simulation setup

In contrast with graphene which is purely sp^2 hybridized, the Si-Si bonding character of buckled silicene is mixed sp^2/sp^3-like. Our MD simulations show that the Si-Si bond length is 2.242 Å and the buckling distance is 0.427 Å, which is comparable with previous *ab initio* calculations [17, 18] and MD simulations [19]. The SNMs were constructed by introducing periodically arranged nanoholes or nanopores in a single layer silicene. The structures of SNMs can be characterized by the indices $\{R, W_x, W_y\}$, where R reflects the size of the nanohole calculated by $N_{\text{removed}}=6R^2$ (N_{removed} is the number of the removed silicon atoms for one nanohole). W_x and W_y indicate the numbers of silicon atoms between the neighboring holes along x- and y-directions, respectively. Fig. 1 depicts an example of {1, 4, 3} SNM.

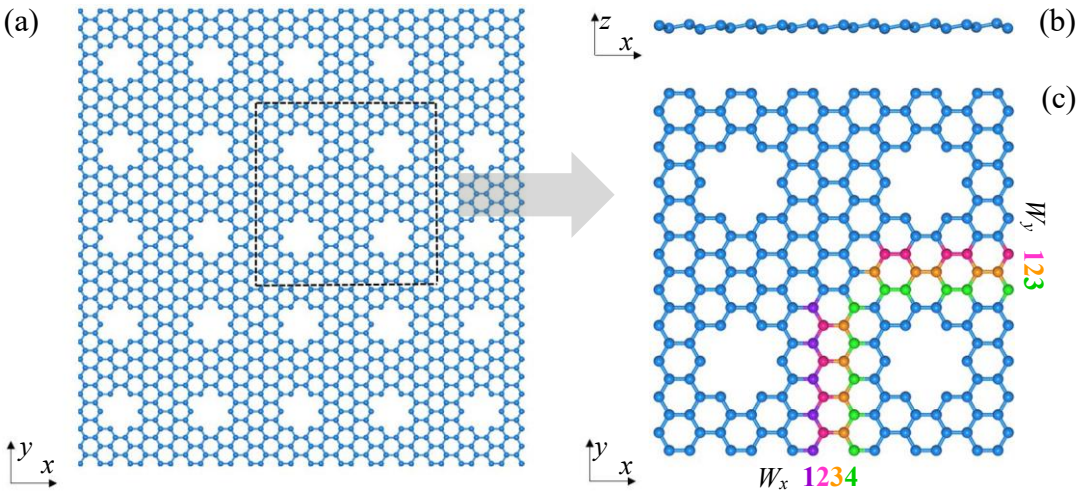

Figure 1. (a) Geometric configuration of SNM. Partial enlarged (b) side and (c) top views of geometric configuration of SNM.

The NEMD method was employed to calculate the thermal conductivity, and it has been

successfully applied to predict the heat-transfer properties of various nanostructures [20-23]. All MD calculations were carried out using LAMMPS [24]. A time step of 0.5 fs was chosen to ensure the accurate and computationally efficient MD simulations. It has been successfully used to study the thermal conductivities of pristine silicene [19] and polycrystalline silicene with vacancy defects [25]. The periodic boundary conditions were applied along the two in-plane directions (i.e., *x*- and *y*-axis), and a free boundary condition was used in the out-of-plane direction (i.e., *z*-axis). The Si-Si bonding interactions were determined by the optimized SW1 potential [19], which can reproduce the low buckled structure of silicene and phonon dispersion curves from *ab initio* calculations. Additional validation of the optimized SW1 potential for SNMs is provided in Supporting Information 1. The system was first relaxed in the NPT ensemble for 0.5 ns, and then equilibrated under the NVT ensemble for 1 ns. Following equilibration, we computed the thermal conductivity using the NEMD method. The last layers of atoms at both system ends were fixed to prevent atoms from sublimating. To create a temperature gradient, two Nosé-Hoover thermostats [26] were applied at the atom layers next to the fixed layers at each end. The system evolved in the NVE ensemble for another 4 ns, in which the last 2 ns was used to obtain the temperature gradient $\partial T/\partial L$ and heat flux q. The thermal conductivity κ was then calculated according to the Fourier's law

$$\kappa = \frac{q}{hw\left(\partial T / \partial L\right)} \tag{1}$$

where w and h (=4.2 Å [27]) are the width and thickness of silicene, respectively.

The final result of thermal conductivity is the mean value of five realizations with

independent initial velocity distributions. The standard deviation of five simulations was calculated to provide the uncertainty in the thermal conductivity result.

3. Results and discussion

3.1 Thermal conductivity

At first, the thermal conductivity of {1, 4, 3} SNM ($\kappa_{nanomesh}$) with length of 70 nm and width of 70 nm was calculated in the temperature range of 100-500 K. For comparison, the thermal conductivity of corresponding silicene ($\kappa_{pristine}$) was also investigated. The results are summarized in Fig. 2(a). The thermal conductivity of silicene at 300 K is about 14.17 $Wm^{-1}K^{-1}$, which agrees well with that obtained previously via the first principles prediction [28]. Fig. 2(a) also shows that the SNM exhibits a decreased thermal conductivity. The reduction ratio of thermal conductivity ($1-\kappa_{nanomesh}/\kappa_{pristine}$) of SNM is smaller than that of GNM. At 300 K, a porosity of about 23.68% (that is the porosity of {1, 4, 3} SNM) yields a reduction ratio of about 72% for SNM and 85~99.5% [14, 15] for GNM. Similar phenomenon is also observed in silicene with isotope substitution. Srinivasan et al. [29] have found that the reduction ratio of thermal conductivity of silicene due to the isotope substitution is small compared to that observed in graphene. In addition, as shown in Fig. 2(a), both the thermal conductivities of silicene and SNM decrease with the increase in temperature, which comes from the stronger anharmonic phonon-phonon scattering at higher temperature [30]. However, the thermal conductivity of SNM decreases much more slowly than that of silicene. This is because the presence of nanoholes turns some delocalized phonon modes into localized phonon modes

(details in Fig. 4). It has been demonstrated that the localized phonon modes can weaken the temperature dependence of thermal conductivity [31, 32], which is also recently observed in the silicon nanotubes [30], crystalline-core/amorphous-shell silicon nanowires [32] and graphene phononic crystal [15].

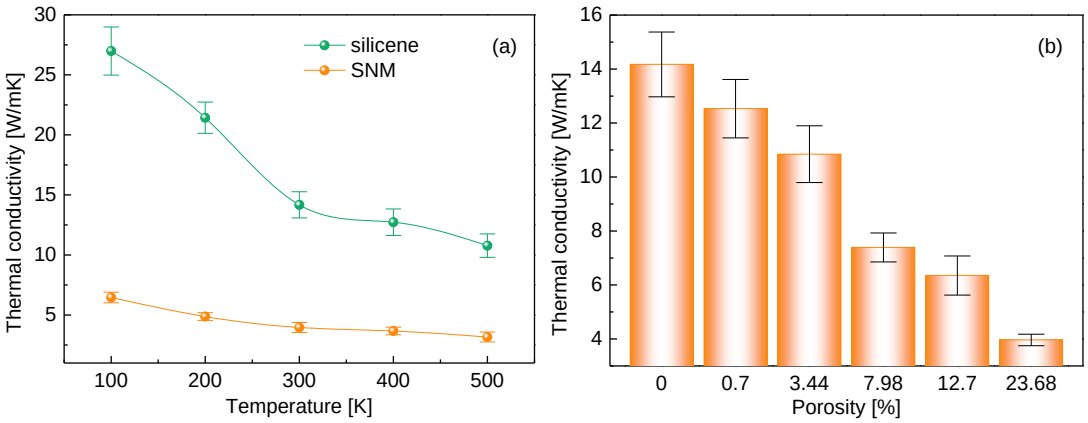

Figure 2. (a) Thermal conductivity of silicene and SNM under different temperatures. (b) Thermal conductivity of SNM under different porosities.

Besides the temperature dependence, the porosity effect on thermal conductivity was investigated. We fixed the length and width of SNM at about 70 nm, and varied the number of nanoholes from 0 to 1225. Each nanohole is formed by removing 6 Si atoms. Accordingly, the total number of removed Si atoms varied from 0 to 7350. The porosity is defined as the ratio of the total area of the nanoholes to the area of silicene. The porosities of SNMs with indices {1, 60, 53}, {1, 24, 21}, {1, 12, 11}, {1, 8, 7} and {1, 4, 3} are about 0.70, 3.44, 7.98, 12.70 and 23.68%, respectively. The simulation results at a temperature of 300 K are shown in Fig. 2(b). As the porosity increases from zero to 23.68%, the thermal conductivity of SNM decreases from 14.17 to 3.96 $Wm^{-1}K^{-1}$. This rapid decay may be attributed to the decrease in the neck width (i.e., the smallest edge-to-edge distance between two adjacent nanoholes) for phonon transport and an

enhancement of boundary scattering. Moreover, we found that the low thermal conductivity of SNM deviates from the Fourier classical Eucken model [33, 34]. The Eucken model is only valid for the structures with size being much longer than the phonon mean free path, and hence is not applicable to SNMs, due to the strong size effect in nanostructures.

3.2 Phonon backscattering

The reduction of SNM thermal conductivity is firstly interpreted by studying phonon backscattering using a temperature distribution analysis. As shown in Fig. 3(a), a 60-nm-long and 10-nm-wide SNM with two nanoholes was selected as a NEMD simulation domain. A 30 K temperature difference was applied to the simulation domain. The NEMD simulation was run for sufficient time (about 2 ns) to obtain the stable system, where the heat flux and temperature distribution are independent of time. The SNM was equally divided into many slabs along the length direction. According to the energy equipartition theorem, the temperatures of these slabs can be calculated as [35]

$$T = \frac{2}{3Nk_{\mathrm{B}}} \sum_{1}^{N} \frac{1}{2} m_i v_i^2 \tag{2}$$

where N is the number of atoms in each slab, k_{B} is the Boltzmann constant, m_i is the mass and v_i is the velocity of the i-th atom.

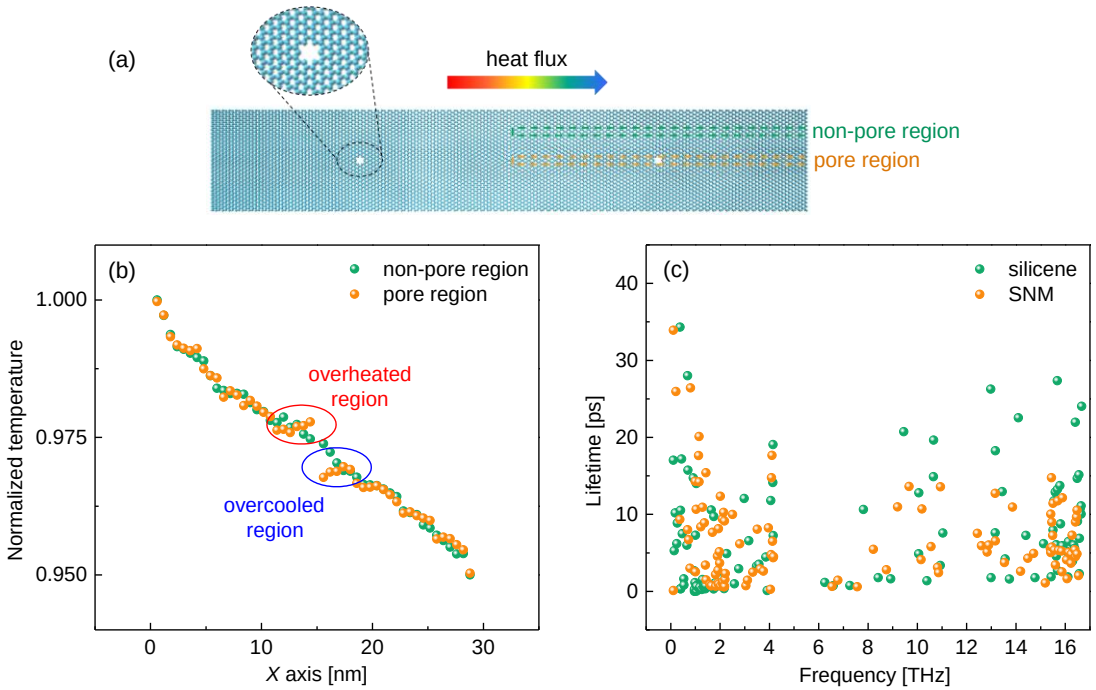

Figure 3. (a) NEMD simulation domain of SNM. (b) Normalized temperature profiles of SNM along the length direction. (c) Phonon lifetimes of silicene and SNM at 300 K.

Fig. 3(b) shows the normalized temperature profiles in the pore and non-pore regions within the dashed lines in Fig. 3(a). It can be seen that the temperature profile in the non-pore region shows nice linearity. Differently, the non-linear temperature distribution is observed in the pore region. Since the neck width of the SNM shown in Fig. 3(a) (about 29.17 nm) is comparable to the phonon mean free path of silicene (approximately 29.30 nm [36]), most phonons propagate ballistically between two neighbouring holes and may get backscattered at hole edges. Accordingly, as shown in Fig. 3(b), there is a locally overheated region near the left edge of the hole due to the phonon backscattering occurring at the hole edges. Similarly, a locally overcooled region exists around the right edge of the hole as it cannot directly receive the hotter phonons from its left neighbouring hole. These two inverted temperature profiles give

rise to an extra thermal resistance, which leads to the reduction in thermal conductivity of SNM. It should be noted that this conclusion is applicable to other SNMs considered in this paper. The neck widths of SNMs with indices {1, 60, 53}, {1, 24, 21}, {1, 12, 11}, {1, 8, 7} and {1, 4, 3} are about 10.09, 4.23, 2.24, 1.57 and 0.90 nm, which are smaller than the phonon mean free path of silicene. Whether the neck width of SNM is smaller than or comparable to the phonon mean free path of silicene, the heat conduction between two adjacent holes contains a major ballistic part. Therefore, there is a locally overheated region in all SNMs considered in this paper because of the backscattered phonons from the hole edges.

3.3 Phonon lifetime

Besides the backscattering that can be seen as a boundary scattering event [37], the heat conduction is SNM is also influenced by the other scattering mechanisms in SNMs. Xie et al. [38] have reported that, in addition to the missing mass and missing linkages, the change of force constant of bonds between the under-coordinated atoms near the nanoholes also results in phonon scattering. More details of under-coordinated atoms and their effect are provided in the Supporting Information 2. The overall strength of phonon scattering in SNMs, including phonon-phonon scattering, phonon-boundary scattering, phonon scattering due to missing mass and linkages, and phonon scattering due to the variation of the force constant of bonds associated with nanoholes, is understood by checking the phonon lifetime. The phonon lifetime can be estimated from the spectral energy density (SED) [36, 39, 40]. More calculation details of phonon

lifetime are provided in the Supporting Information 3.

The obtained phonon lifetimes (τ) are presented in Fig. 3(c) as a function of frequency (ω) for both silicene and {1, 4, 3} SNM at 300 K. The lifetime values of silicene are of the same order of magnitude as those obtained in the first-principles investigation [41]. Moreover, it can be seen the general trend of phonon lifetime of silicene is different from that of bulk silicon, which has a $\tau \sim \omega^{-2}$ to $\tau \sim \omega^{-4}$ dependence [42]. Similar results have been obtained in previous studies on silicene [36, 41, 43] and graphene [44]. After introducing nanoholes, the lifetimes are reduced for the high frequency range. The lifetime attenuation stems from the phonon scatterings occurring at the nanohole edges. One can expect that phonon modes with shorter wavelengths (i.e. higher frequencies) are more sensitive to the nanoholes in SNM than those with larger wavelengths (i.e. lower frequencies). The lifetime attenuation of high-frequency phonons helps to explicitly explain the lower thermal conductivity of SNM.

3.4 Phonon localization

To gain a better insight for thermal conductivity suppression, the phonon participation ratio (PR) [45, 46] is calculated to analyze the phonon localization. The PR, defined as

$$\mathrm{PR}_{\lambda}^{-1} = N\sum_{i}\left(\sum_{\alpha}\varepsilon_{i\alpha,\lambda}^{*}\varepsilon_{i\alpha,\lambda}\right)^{2} \tag{3}$$

indicates the fraction of atoms participating in a given mode λ. N is the total number of atoms, i sums over all the atoms, α is a Cartesian direction and sums over x, y, z , and $\varepsilon_{i\alpha,\lambda}$ is the vibrational eigenvector component corresponding to the λ-th normal mode, superscript * denotes the complex conjugate. When there are less atoms participating

in the motion, the phonon mode has a smaller PR value [47]. For instance, PR is 1 when all atoms participate in the motion. When only one atom vibrates in the localized mode, PR is calculated out as 1/*N*. That is, a smaller PR value corresponds to the more localized phonon mode.

The PR of all modes in the spectrum for silicene and SNMs with different porosities are shown in Fig. 4. It can be seen from Fig. 4(a) that the values of PR in silicene split into two parts: one part is in the range of 0.27-0.46; the other part resides in a lower range of 0.03-0.27. This result is fundamentally different from graphene, whose PR values are almost uniformly distributed [14, 15]. The layered PR may be related to the low buckled structure of silicene, which is made of sp^2-bonded and sp^3-like-bonded silicon atoms. As shown in Fig. 4(b) and (c), the introduction of nanopores results in a more uniform distribution of PR values. In addition, the values of PR in SNM are smaller than those in silicene throughout the whole frequency range. That is, the phonon modes in SNMs are likely localized. When a silicene sheet is patterned into a SNM, the hole edges are generated. The phonon localization in SNM may be related to the localized edge modes [48, 49], whose localization origins from the edge configuration and core is the edge atoms. The vibrational amplitude of the localized edge modes decreases to zero very quickly from edges into center [45, 46]. Since the localized modes are less effective in transporting thermal energy than the delocalized modes [30, 50], it follows that the lower thermal conductivity of SNM must be expected. By comparing Fig. 4(b) with 4(c), we find that there is a reduction of the PR in SNM when the porosity changes from 12.70 to 23.68%, which indicates that the phonon localization in SNM is enhanced at

large porosity. It may help to explain the results in Fig. 2(b) that the SNM with larger porosity presents a lower thermal conductivity.

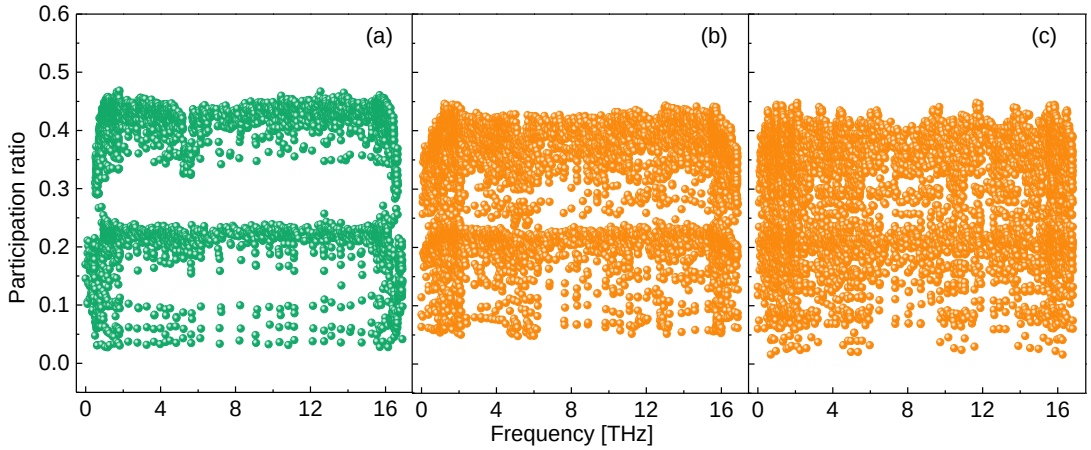

Figure 4. Participation ratios for (a) pristine silicene, (b) SNM with 12.70% porosity and (c) SNM with 23.68% porosity.

3.5 Phonon coherent resonance

SNMs can be viewed as 2-D superlattices constructed by periodically arranged nanopores, in which the coherent phonon transport is of great interest. To further analyze the phonon coherence in SNMs, we evaluated the mode weight factor (MWF), which is calculated as [51, 52]

$$\mathrm{MWF}_{j',\lambda} = \sum_{j'} \sum \alpha \left(\varepsilon_{ja,\lambda} \right)^2 \tag{4}$$

where the prime means that sum over j (atoms) and is exclusively restricted to the in-plane or the out-of-plane buckling regions (see Fig. 5(a)). Therefore, the sum of MWFs in the whole silicene sheet should be equal to 1. That is, $\mathrm{MWF}_{\text{in-plane},\lambda} + \mathrm{MWF}_{\text{out-of-plane},\lambda} = 1$. Any change in one component causes an adverse change in the other.

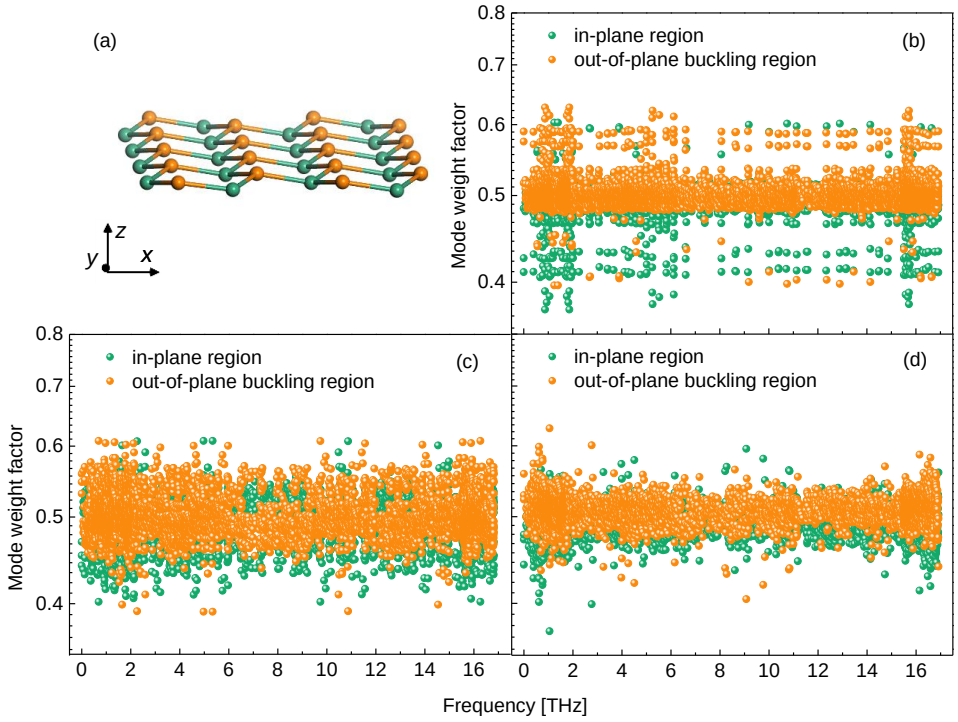

Figure 5. (a) The partial structure of silicene. The green and orange atoms represent the in-plane and the out-of-plane buckling regions, respectively. Participation ratios for (b) silicene, (c) SNM with 12.70% porosity and (d) SNM with 23.68% porosity.

The MWFs of silicene and SNMs with different porosities are shown in Fig. 5(b)-(d). For silicene, as can be seen in Fig. 5(b), the MWF of out-of-plane buckling region is larger than that of in-plane region. This observation suggests that the vibrations of Si atoms in the out-of-plane buckling region have a greater contribution to the heat transfer of silicene. Fig. 5(c) and (d) show that the MWFs of SNMs have different features. The nanopores induce the decrease in MWF of out-of-plane buckling region while increase in MWF of in-plane region. The MWFs of the in-plane and the out-of-plane buckling regions approach each other, and are approximately equal at large porosity. In other words, for each phonon modes, all of the atoms from the in-plane and the out-of-plane buckling regions participate and vibrate with the same frequency. They contribute

equally to the total vibration and the phonon modes exhibit coherent resonant behavior. As reported in graphyne nanotubes [53] and Si-based nanophononic materials [54, 55] previously, the coherent resonant behavior of phonons is believed to reduce the phonon group velocities and consequently leads to a reduction in thermal conductivity.

4. Conclusions

Nonequilibrium molecular dynamics simulations were employed to study the thermal conductivity of SNMs. The simulation results demonstrate that the thermal conductivity of SNM is much lower than that of pristine silicene. Moreover, the thermal conductivity of SNM decreases with the increasing porosity, and has a weak temperature dependence. By analyzing the temperature distribution, phonon lifetime, phonon participation ratio and mode weight factor, both coherent and incoherent phonon transport in SNMs were investigated. It is found that the introduction of nanoholes induces the phonon backscattering, phonon localization and phonon coherent resonance, which results in the reduction in SNM thermal conductivity. This study provides a felicitous reference for further investigations on modifying thermal properties of silicene.

Acknowledgements

This work is supported by the National Natural Science Foundation of China (No. 51806064, 51741604, 51676069 and 51776066), China Postdoctoral Science Foundation Funded Project (No. 2016M600980), Hong Kong Scholars Program (No. XJ2016042), and Fundamental Research Funds for the Central Universities (No.

2018QN047 and 2015ZZD09).

References

1. K. S. Novoselov, A. K. Geim, S. V. Morozov, D. Jiang, Y. Zhang, S. V. Dubonos, I. V. Grigorieva and A. A. Firsov, *Science*, 2004, 306, 666-669.
2. S. Ghosh, I. Calizo, D. Teweldebrhan, E. P. Pokatilov, D. L. Nika, A. A. Balandin, W. Bao, F. Miao and C. N. Lau, *Applied Physics Letters*, 2008, 92, 151911.
3. A. A. Balandin, *Nature Materials*, 2011, 10, 569-581.
4. M. Xu, T. Liang, M. Shi and H. Chen, *Chemical Reviews*, 2013, 113, 3766-3798.
5. S. Z. Butler, S. M. Hollen, L. Cao, Y. Cui, J. A. Gupta, H. R. Gutiérrez, T. F. Heinz, S. S. Hong, J. Huang and A. F. Ismach, *ACS Nano*, 2013, 7, 2898-2926.
6. L. C. L. Yan Voon and G. G. Guzmán-Verri, *MRS Bulletin*, 2014, 39, 366-373.
7. A. Dimoulas, *Microelectronic Engineering*, 2015, 131, 68-78.
8. M. Ali, X. Pi, Y. Liu and D. Yang, *AIP Advances*, 2017, 7, 045308.
9. G. G. Guzmán-Verri and L. L. Y. Voon, *Physical Review B*, 2007, 76, 075131.
10. T. Jia, X. Fan, M. Zheng and G. Chen, *Scientific Reports*, 2016, 6, 20971.
11. L. Gong, S. Xiu, M. Zheng, P. Zhao, Z. Zhang, Y. Liang, G. Chen and Y. Kawazoe, *Journal of Materials Chemistry C*, 2014, 2, 8773-8779.
12. H. Şahin and S. Ciraci, *Physical Review B*, 2011, 84, 035452.
13. X. Liang, Y. S. Jung, S. Wu, A. Ismach, D. L. Olynick, S. Cabrini and J. Bokor, *Nano Letters*, 2010, 10, 2454-2460.
14. T. Feng and X. Ruan, *Carbon*, 2016, 101, 107-113.
15. L. Yang, J. Chen, N. Yang and B. Li, *International Journal of Heat and Mass Transfer*, 2015, 91, 428-432.
16. M. Yarifard, J. Davoodi and H. Rafii-Tabar, *Computational Materials Science*, 2016, 111, 247-251.
17. S. Cahangirov, M. Topsakal, E. Aktürk, H. Şahin and S. Ciraci, *Physical Review Letters*, 2009, 102, 236804.
18. Z. Ni, Q. Liu, K. Tang, J. Zheng, J. Zhou, R. Qin, Z. Gao, D. Yu and J. Lu, *Nano Letters*, 2011, 12, 113-118.
19. X. Zhang, H. Xie, M. Hu, H. Bao, S. Yue, G. Qin and G. Su, *Physical Review B*, 2014, 89, 054310.
20. L. Cui, Y. Zhang, X. Du and G. Wei, *Journal of Materials Science*, 2018, 53, 4242-4251.
21. R. Rurali, L. Colombo, X. Cartoixa, Ø. Wilhelmsen, T. T. Trinh, D. Bedeaux and S. Kjelstrup, *Physical Chemistry Chemical Physics*, 2016, 18, 13741-13745.
22. L. Xu, X. Zhang and Y. Zheng, *Physical Chemistry Chemical Physics*, 2015, 17, 12031-12040.
23. L. Cui, X. Du, G. Wei and Y. Feng, *The Journal of Physical Chemistry C*, 2016, 120, 23807-23812.

24. S. Plimpton, *Journal of Computational Physics*, 1995, 117, 1-19.
25. Y. Gao, Y. Zhou, X. Zhang and M. Hu, *The Journal of Physical Chemistry C*, 2018, 122, 9220-9228.
26. D. Frenkel and B. Smit, *Understanding molecular simulation: from algorithms to applications*, Academic Press, 2001.
27. M. Hu, X. Zhang and D. Poulikakos, *Physical Review B*, 2013, 87, 195417.
28. X. Gu and R. Yang, *Journal of Applied Physics*, 2015, 117, 025102.
29. S. Srinivasan, U. Ray and G. Balasubramanian, *Chemical Physics Letters*, 2016, 650, 88-93.
30. J. Chen, G. Zhang and B. Li, *Nano Letters*, 2010, 10, 3978-3983.
31. J. L. Feldman, M. D. Kluge, P. B. Allen and F. Wooten, *Physical Review B*, 1993, 48, 12589.
32. D. Donadio and G. Galli, *Nano Letters*, 2010, 10, 847-851.
33. D. Song and G. Chen, *Applied Physics Letters*, 2004, 84, 687-689.
34. J. Tang, H. Wang, D. H. Lee, M. Fardy, Z. Huo, T. P. Russell and P. Yang, *Nano Letters*, 2010, 10, 4279-4283.
35. X. Wang, M. Wang, Y. Hong, Z. Wang and J. Zhang, *Physical Chemistry Chemical Physics*, 2017, 19, 24240-24248.
36. Z. Wang, T. Feng and X. Ruan, *Journal of Applied Physics*, 2015, 117, 084317.
37. J. Lee, W. Lee, G. Wehmeyer, S. Dhuey, D. L. Olynick, S. Cabrini, C. Dames, J. J. Urban and P. Yang, *Nature Communications*, 2017, 8, 14054.
38. G. Xie, Y. Shen, X. Wei, L. Yang, H. Xiao, J. Zhong and G. Zhang, *Scientific Reports*, 2014, 4.
39. J. A. Thomas, J. E. Turney, R. M. Iutzi, C. H. Amon and A. J. McGaughey, *Physical Review B*, 2010, 81, 081411.
40. T. Feng, X. Ruan, Z. Ye and B. Cao, *Physical Review B*, 2015, 91, 224301.
41. H. Xie, M. Hu and H. Bao, *Applied Physics Letters*, 2014, 104, 131906.
42. K. Esfarjani, G. Chen and H. T. Stokes, *Physical Review B*, 2011, 84, 085204.
43. X. Zhang, H. Bao and M. Hu, *Nanoscale*, 2015, 7, 6014-6022.
44. B. Qiu and X. Ruan, *Applied Physics Letters*, 2012, 100, 193101.
45. R. J. Bell and P. Dean, *Discussions of the Faraday Society*, 1970, 50, 55-61.
46. A. Bodapati, P. K. Schelling, S. R. Phillpot and P. Keblinski, *Physical Review B*, 2006, 74, 245207.
47. L. Yang, N. Yang and B. Li, *Nano Letters*, 2014, 14, 1734-1738.
48. J. Jiang, J. Chen, J. Wang and B. Li, *Physical Review B*, 2009, 80, 052301.
49. J. Jiang and J. Wang, *Physical Review B*, 2010, 81, 174117.
50. M. Hu, K. P. Giapis, J. V. Goicochea, X. Zhang and D. Poulikakos, *Nano Letters*, 2010, 11, 618-623.
51. X. Zhang, M. Hu, K. P. Giapis and D. Poulikakos, *Journal of Heat Transfer*, 2012, 134, 102402.
52. J. L. Feldman and N. Bernstein, *Physical Review B*, 2004, 70, 235214.
53. X. Chen, C. Chen, J. Liu and K. Chen, *Journal of Physics D: Applied Physics*, 2017, 50, 345301.
54. H. Honarvar and M. I. Hussein, *Physical Review B*, 2016, 93, 081412.

55. S. Xiong, K. Sääskilahti, Y. A. Kosevich, H. Han, D. Donadio and S. Volz, *Physical Review Letters*, 2016, 117, 025503.